

Excellence in Chemistry Research

Announcing our new flagship journal

- Gold Open Access
- Publishing charges waived
- Preprints welcome
- Edited by active scientists



Meet the Editors of *ChemistryEurope*



Luisa De Cola

Università degli Studi
di Milano Statale, Italy



Ive Hermans

University of
Wisconsin-Madison, USA



Ken Tanaka

Tokyo Institute of
Technology, Japan

Selective Chelation of the Exotic Meitner-Auger Emitter Mercury-197 m/g with Sulfur-Rich Macrocyclic Ligands: Towards the Future of Theranostic Radiopharmaceuticals

Parmissa Randhawa,^[a, b] K. Lexi Gower-Fry,^[a, b] Cailum M. K. Stienstra,^[b] Marianna Tosato,^[a, b, c] Shaohuang Chen,^[a, b] Yang Gao,^[d, e] Anthony W. McDonagh,^[a] Valerio Di Marco,^[c] Valery Radchenko,^[b, f] Georg Schreckenbach,^[d] and Caterina F. Ramogida^{*[a, b]}

Abstract: Mercury-197 m/g are a promising pair of radioactive isomers for incorporation into a *theranostic* as they can be used as a diagnostic agent using SPECT imaging and a *therapeutic* via Meitner-Auger electron emissions. However, the current absence of ligands able to stably coordinate ^{197m/9}Hg to a tumour-targeting vector precludes their use in vivo. To address this, we report herein a series of sulfur-rich chelators capable of incorporating ^{197m/9}Hg into a radiopharmaceutical. 1,4,7,10-Tetrathia-13-azacyclopentadecane (NS₄) and its derivatives, (2-(1,4,7,10-tetrathia-13-azacyclopentadecan-13-yl)acetic acid (NS₄-CA) and *N*-benzyl-2-(1,4,7,10-tetrathia-13-azacyclopentadecan-13-yl)acetamide (NS₄-BA), were designed, synthesized and analyzed for their ability to coordinate Hg²⁺ through a combination of theoretical (DFT) and experimental coordination chemistry studies (NMR and mass spectrometry) as well as ^{197m/9}Hg radiolabeling studies and in vitro stability assays. The development of stable ligands for ^{197m/9}Hg reported herein is extremely impactful as it would enable their use for in vivo imaging and therapy, leading to personalized treatments for cancer.

tadecan-13-yl)acetic acid (NS₄-CA) and *N*-benzyl-2-(1,4,7,10-tetrathia-13-azacyclopentadecan-13-yl)acetamide (NS₄-BA), were designed, synthesized and analyzed for their ability to coordinate Hg²⁺ through a combination of theoretical (DFT) and experimental coordination chemistry studies (NMR and mass spectrometry) as well as ^{197m/9}Hg radiolabeling studies and in vitro stability assays. The development of stable ligands for ^{197m/9}Hg reported herein is extremely impactful as it would enable their use for in vivo imaging and therapy, leading to personalized treatments for cancer.

Introduction

The academic and clinical interest in radiopharmaceutical development has grown tremendously over the past decades. These radioactive drugs can diagnose (via molecular imaging) and provide potent, targeted therapies (via targeted radionuclide therapy – TRT) for some of medicine’s most challenging diseases, such as cancer and infection.^[1] Depending on the emissions released following radioactive decay, these radio-labelled drugs can be exploited for TRT (via emission of alpha (α), beta (β^-) particles, or Meitner-Auger electrons – MAEs) or molecular imaging (via emission of positrons (β^+) for positron emission tomography (PET), or gamma (γ) rays for single-photon emission computed tomography (SPECT)).^[2] While the majority of research and clinical efforts have focused on employing β^- or α -emitting radionuclides for therapy,^[3,4] MAE-emitting nuclides remain rather unexplored. MAEs are unique since they can offer the most localized dose of ionizing radiation ($< 1 \mu\text{m}$) compared to their β^- or α -emitting counterparts (0.05–12 mm and 50–100 μm , respectively); they also possess a high linear energy transfer (LET; 4–26 keV/ μm) implicating their high cytotoxic potential.^[5–13]

In recent years, the term *theranostic* or *radio-theranostic* has been coined for radiopharmaceuticals which can be used for combined diagnostic and *therapeutic* purposes by using the same construct radiolabeled first with a nuclide that emits γ -rays to diagnose and stage disease, followed by a nuclide that emits cytotoxic particles to treat subsequently.

Mercury-197 m (^{197m}Hg, $t_{1/2} = 23.8 \text{ h}$) and mercury-197 g (^{197g}Hg, $t_{1/2} = 64.1 \text{ h}$) are a promising unconventional radiometal pair for incorporation into a “same-element” theranostic agent

[a] P. Randhawa, K. L. Gower-Fry, Dr. M. Tosato, S. Chen, Dr. A. W. McDonagh, Prof. Dr. C. F. Ramogida
Department of Chemistry
Simon Fraser University
8888 University Drive, V5A 1S6 Burnaby, British Columbia (Canada)
E-mail: cfr@sfu.ca
Homepage: <https://www.sfu.ca/chemistry/department/faculty-staff/profiles/research-faculty/cfr.html>


[b] P. Randhawa, K. L. Gower-Fry, C. M. K. Stienstra, Dr. M. Tosato, S. Chen, Dr. V. Radchenko, Prof. Dr. C. F. Ramogida
Life Sciences Division, TRIUMF
4004 Wesbrook Mall, V6T 2A3 Vancouver, British Columbia (Canada)


[c] Dr. M. Tosato, Prof. Dr. V. Di Marco
Department of Chemical Sciences
University of Padova
via Marzolo 1, 35131 Padova (Italy)

[d] Dr. Y. Gao, Prof. Dr. G. Schreckenbach
Department of Chemistry
University of Manitoba
140 Dysart Rd, R3T 2N2 Winnipeg, Manitoba (Canada)

[e] Dr. Y. Gao
Institute of Fundamental and Frontier Sciences
University of Electronic Science and Technology of China
610054 Chengdu, Sichuan (P. R. China)

[f] Dr. V. Radchenko
Department of Chemistry
University of British Columbia
2036 Main Mall, V6T 1Z1 Vancouver, British Columbia (Canada)

 Supporting information for this article is available on the WWW under <https://doi.org/10.1002/chem.202203815>

 © 2023 The Authors. Chemistry - A European Journal published by Wiley-VCH GmbH. This is an open access article under the terms of the Creative Commons Attribution Non-Commercial License, which permits use, distribution and reproduction in any medium, provided the original work is properly cited and is not used for commercial purposes.

since the former emits γ -rays ($E_\gamma = 133.98$ keV, $I_\gamma = 34.8\%$ and $E_\gamma = 278.65$ keV, $I_\gamma = 3.79\%$) compatible with SPECT, while both release a cascade of conversion electrons – CE (average yield/decay = 2.4), and MAEs (average yield/decay = 42.6) that can be used for therapy.^[5,6,13–18]

^{197m}gHg was first employed in nuclear medicine when it was incorporated into 3-chloromercury-2-methoxyprop-1-yl (chlormerodrin) (Figure 1A) in the mid-1960s for use as a SPECT imaging agent for brain scanning.^[19–22] Due to isotope purity issues, its use was discontinued in the early 1970s and replaced with the SPECT imaging isotope technetium-99 m (^{99m}Tc).^[19,22–24] Recent improvements towards the production of high specific activity ^{197m}gHg has spurred renewed interest in this isomeric pair. Gilpin et al. studied the incorporation of ^{197m}gHg via organometallic bonds using a cyclic bisarylmercury complex (Figure 1B), which showed good organ clearance and no retention in the kidney in a biodistribution study, indicating the complex may be stable in vivo, while Pietzsch et al. reported a variety of ^{197m}gHg labelled organic molecules (Figure 1C) obtained via electrophilic substitution to produce in vivo stable compounds.^[25,26]

Unlike the majority of previous work, which incorporates ^{197m}gHg via organometallic bonds, this work aims to incorporate this theranostic pair into a radiopharmaceutical via the bifunctional chelator (BFC) approach.^[2,5,19,20,23,25,26,28] BFCs link the radioisotope to a disease-specific targeting vector allowing selective and targeted delivery of the radiation payload to diseased cells.^[1,13,29,30] The BFC method in inorganic radiopharmaceutical design is attractive since all the synthesis of the chelate and biomolecule occurs before the addition of the radionuclide, enabling a 1-step labeling process, saving many half-lives of radioactivity.^[2] Moreover, this approach enables facile implementation in clinical settings with ‘kit’ type labeling. For these reasons, we believe that the BFC approach will be essential to fully exploit the theranostic potential of ^{197m}gHg .

In designing a BFC, characteristics such as the coordination chemistry of the radiometal, the kinetics of complexation, and the selectivity of the chelator to other metals should be considered. Ideally, the BFC should exhibit rapid and quantitative radiometal complexation under favourable radiochemical conditions (i.e., mild reaction temperatures, physiological pH, and sub-micromolar chelator concentrations).^[14,31] These properties should guarantee a high molar activity of the radioligand since high concentrations of unlabelled chelator/bioconjugate might compromise its diagnostic or therapeutic efficacy.^[1,2]

Moreover, it is imperative that the resulting radiometal-complex be thermodynamically stable and kinetically inert to prevent dissociation (e.g., transchelation and metal-exchange reactions) in vivo. This undesired phenomenon would result in high background activity levels and unintended radiation burden to off-target tissue.^[32]

Existing examples of BFCs employed for ^{197m}gHg -complexation are scarce. To the best of our knowledge, at the time of this writing, only a few ^{197m}gHg -radiolabelled macrocycles have been reported in the literature (Figure 1D). Still, none have been reported to be stable in vitro or in vivo.^[27,33] Our objective herein was to develop suitable ligand frameworks that can act as BFCs to form sufficiently stable $^{197m}\text{gHg}^{2+}$ complexes under in vivo conditions; the identification of such frameworks would open up the door to study and fully exploit ^{197m}gHg for radiotheranostic applications, as no suitable BFCs have been identified thus far.

To date, the majority of chelators in radiopharmaceutical design exploit hard O and borderline N donor atoms (i.e., 1,4,7,10-tetraazacyclododecane-1,4,7,10-tetraacetic acid; DOTA) (Figure 2), which do not adequately match the coordination preferences of the soft Lewis acid Hg^{2+} according to Pearson’s Hard-Soft Acid-Base (HSAB) theory. Our research focuses on developing chelators containing soft Lewis base donor atoms (i.e., sulfur) to fulfil the chelation preferences of $^{197m}\text{gHg}^{2+}$. The well-developed Hg^{2+} environmental sensing literature inspired our chelator design. We hypothesized that the 15-member 1,4,7,10-tetrathia-13-azacyclopentadecane macrocycle backbone (NS_4 ; Figure 2), previously developed by Chen et al. and Isaad and Archri as a highly selective and sensitive Hg^{2+} sensing ligand,^[34,35] would make an ideal platform for ^{197m}gHg -based radiopharmaceuticals. This macrocyclic structure was also chosen since it should confer high stability and inertness of the resulting Hg^{2+} -complex due to the macrocyclic effect. Additionally, the secondary amine on the backbone can serve as a convenient location for derivatization and bioconjugation to targeting vectors.

Herein, we report the synthesis, characterization, and non-radioactive Hg^{2+} ($^{\text{nat}}\text{Hg}^{2+}$) complexation of NS_4 and two novel NS_4 derivatives, namely 2-(1,4,7,10-tetrathia-13-azacyclopentadecan-13-yl)acetic acid ($\text{NS}_4\text{-CA}$) and *N*-benzyl-2-(1,4,7,10-tetrathia-13-azacyclopentadecan-13-yl)acetamide ($\text{NS}_4\text{-BA}$) (Figure 2), where the functionalization of the secondary amine mimics the effect that the introduction of a bifunctional handle on the macrocycle would impose on $[\text{Hg}^{2+}]\text{Hg}^{2+}/^{\text{nat}}\text{Hg}^{2+}$ chelation.

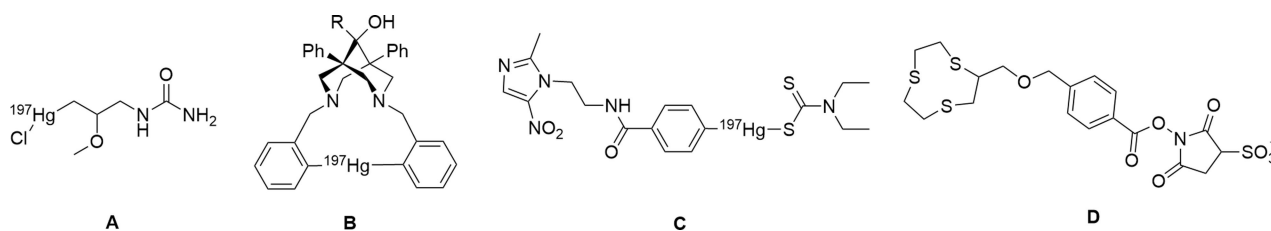


Figure 1. Structure of **A**) chlormerodrin,^[19–21] **B**) and **C**) ^{197m}gHg organometallic compounds developed for radiopharmaceutical incorporation by Gilpin et al. and Pietzsch et al.^[25,26] **D**) bifunctional trithiamacrocycle reported by Blower et al.^[27]

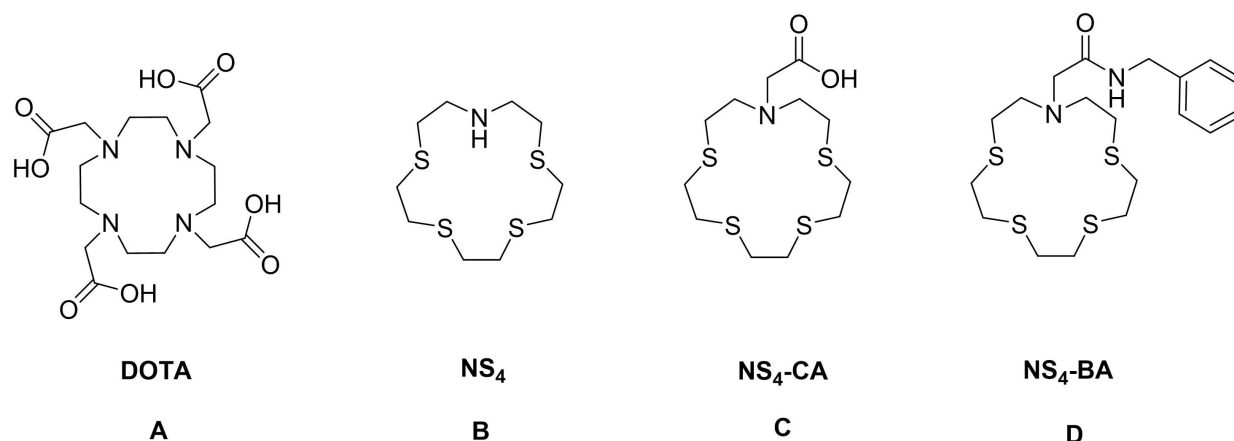


Figure 2. Structures of the ligands investigated in this work with $[^{197m/g}\text{Hg}]\text{Hg}^{2+}/^{\text{nat}}\text{Hg}^{2+}$: A) DOTA, B) NS₄, C) NS₄-CA and D) NS₄-BA.

The $^{\text{nat}}\text{Hg}^{2+}$ coordination chemistry was explored via 1D and 2D NMR, HR/LR ESI-MS, and DFT calculations to understand the critical components of the BFC that affect metal-ligand binding.^[36] The ligands were also investigated for their ability to complex $[^{197m/g}\text{Hg}]\text{Hg}^{2+}$ via radiolabeling studies and compared to the commercial standard in radiometal chelation (DOTA).^[37] Furthermore, the radiometal-complex stability was assessed in vitro via human serum and glutathione competition assays to predict the fate of the metal-ligand complexes in vivo. Due to the lack of available literature on $^{197m/g}\text{Hg}$ radiopharmaceuticals, novel radiolabeling and stability protocols were established.

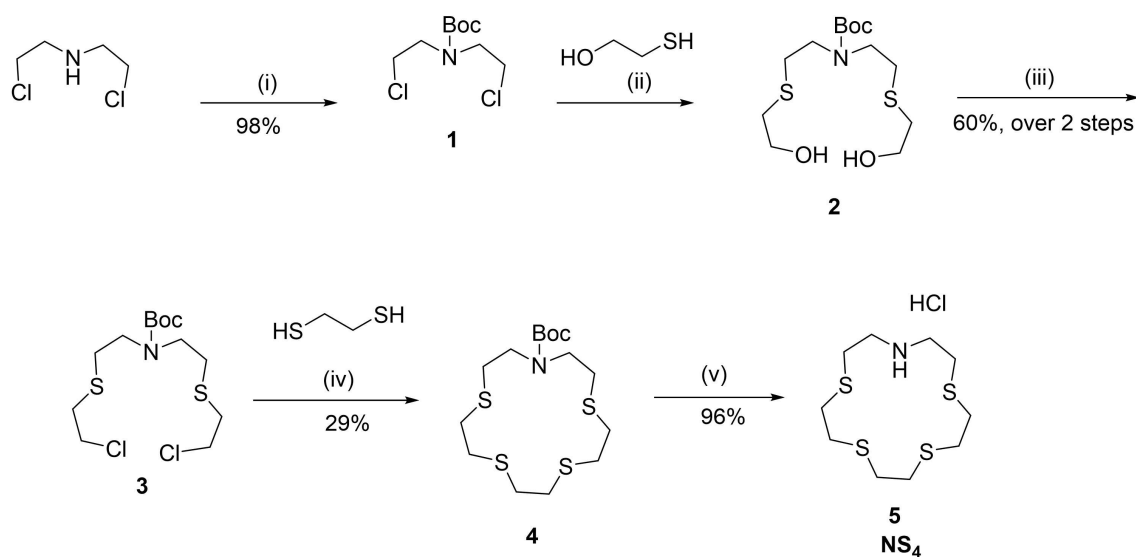
Results and Discussion

Synthesis and characterization of NS₄ ligand series

The NS₄ macrocyclic ligand backbone **5** has been previously synthesized and reported in the literature as a highly selective chelator for Hg²⁺ with potential use in chemosensor applications when attached to a fluorophore.^[34] Therefore, we hypothesized herein that this platform could make an appropriate scaffold for $^{197m/g}\text{Hg}$ chelation with the possibility to be used in cutting-edge Hg²⁺-based radiopharmaceuticals.

An adapted synthesis of the NS₄ macrocycle was developed herein by combining and modifying reaction conditions of two previously reported procedures (Scheme 1).^[35,38]

An imperative component of a BFC is the integrated reactive moiety allowing for the attachment of the radiometal



Scheme 1. Synthesis of NS₄. Reagents and conditions: i) CH₂Cl₂, 10% NaOH, di-tert-butyl dicarbonate, RT, 23 h; ii) DMF, 2-mercaptoethanol, K₂CO₃, 40 °C, 69 h; iii) CH₂Cl₂, TEA, tosyl chloride, RT, 22 h; iv) DMF, KI, Cs₂CO₃, 1,2-ethanedithiol, 50 °C, 48 h; v) CH₃OH, EtOAc, HCl, 45 °C, 24 h. The overall yield for the backbone synthesis was calculated to be 16%.

complex to the tumour targeting vector. Different strategies are used for bioconjugation. Most commonly, the BFC connected with a linker reacts with available primary amines on the bioactive molecules. The NS₄ macrocycle studied herein permits a straightforward path to bifunctionalization via alkylation of the secondary amine, as such, an activated carbonyl derivative (**8**) was synthesized.^[1] In order to assess the impact of the bifunctional handle on radiometal chelation, **8** was coupled with benzylamine to give **9**, which acts as a placeholder for future biomolecules.

Synthesis of NS₄-BA (**9**, Scheme 2) was completed through alkylation of the secondary amine of **5** with the *t*-butyl acetate group (yield 64%), following deprotection of **6** with TFA-CH₂Cl₂ (1:1) to obtain the carboxylic acid analogue (NS₄-CA, **7**) with a yield of 84%. Subsequently, **7** underwent *N*-hydroxysuccinimide coupling to give the activated carbonyl (**8**) in an 85% yield. Further reaction of **8** with benzylamine yielded the benzyl amide derivative (NS₄-BA, **9**) with 49% yield. The successful synthesis of **8** and **9** suggests that the conjugation of a targeting vector bearing a primary amine can be successfully achieved.

NS₄, NS₄-CA and NS₄-BA were fully characterized by ¹H, ¹³C{¹H} Nuclear Magnetic Resonance (NMR) spectroscopy and High-Resolution or Low Resolution Electrospray Ionization Mass Spectrometry (ESI-HRMS or LR-MS) (Figures S1–18).

Since metal coordination and protonation processes are concurrent and competitive events, knowing the acid-base equilibria of a chelator is essential in evaluating its complexation ability. Therefore, the acidity constant (p*K*_a) of the secondary amine of the macrocyclic ring of NS₄ was determined via ¹H NMR at 25 °C in 0.1 M NaNO₃ by following the chemical shifts variation of the SCH₂ and NCH₂ protons as a function of pH (Figure S19). Both gave nearly identical p*K*_a values equal to

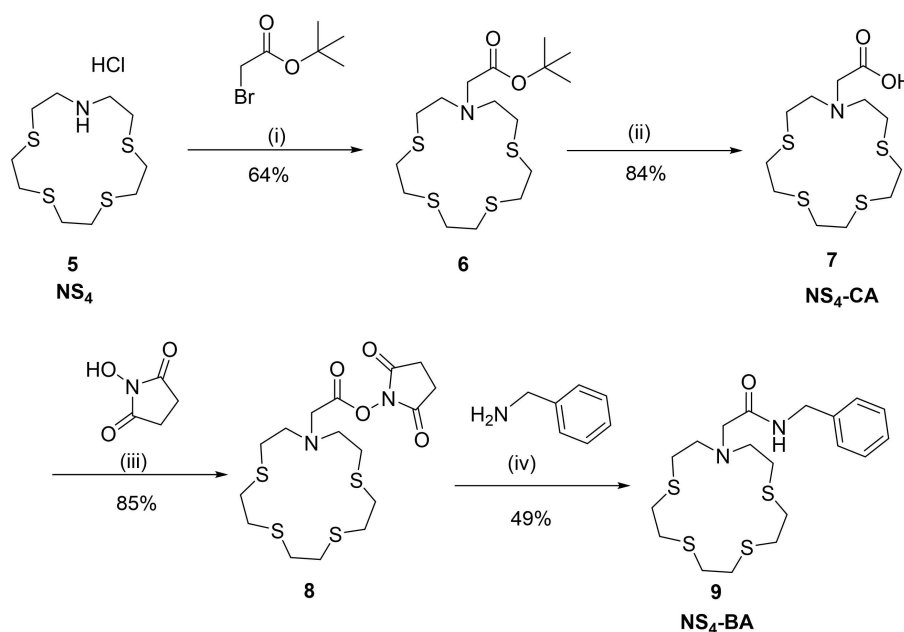
8.23 ± 0.04 and 8.27 ± 0.02, respectively. These values are in reasonable agreement with previously reported p*K*_as for secondary amines.^[39]

Synthesis and characterization of non-radioactive Hg²⁺-complexes

To gain insight into the ability of the NS₄ ligand series to effectively coordinate Hg²⁺, prior to the labeling investigation, complexation studies with non-radioactive Hg²⁺ were conducted. [Hg(NS₄)]²⁺ was prepared by the addition of the metal ion to an aqueous solution of the ligand in equimolar amount, at variable pH for NMR titrations. Alternatively, the Hg²⁺ complexes of NS₄, NS₄-CA, and NS₄-BA were prepared by precipitation in non-aqueous solvent, isolated by centrifugation and dissolved in DMSO. All complexes were then characterized in solution by NMR and HRMS or LRMS.

The latter technique revealed the presence of the characteristic isotope distribution pattern for ^{nat}Hg²⁺-containing compounds, thus confirming the presence of Hg²⁺ complexes having 1:1 metal-to-ligand stoichiometry, namely [Hg(NS₄)]²⁺ (**10**), [Hg(NS₄-CA)]⁺ (**11**) and [Hg(NS₄-BA)]²⁺ (**12**) (Figures S28–30).

The ¹H NMR spectra of the ^{nat}Hg²⁺-complexes in DMSO (Figure 3) unveil that, upon complexation, the resonances with respect to the free ligand undergo downfield shifting. This is common in metal-ligand complexes due to the electron-withdrawing effects of the metal. As all the peaks experienced this shift, it can be concluded that all the donor atoms are involved on average in the metal coordination sphere. The complexation event results in significant broadening of the peaks, which would indicate a fluxional solution behavior occurring on the



Scheme 2. Synthesis of NS₄-CA and NS₄-BA. Reagents and conditions: i) CH₃CN, K₂CO₃, NaI, tert-butyl bromoacetate, RT, 24 h; ii) TFA/CH₂Cl₂ (1:1), RT, 4 h; iii) DMF, *N*-hydroxysuccinimide, EDC, RT, 48 h; iv) CH₂Cl₂, benzylamine, DIPEA, 0 °C – RT, 24 h.

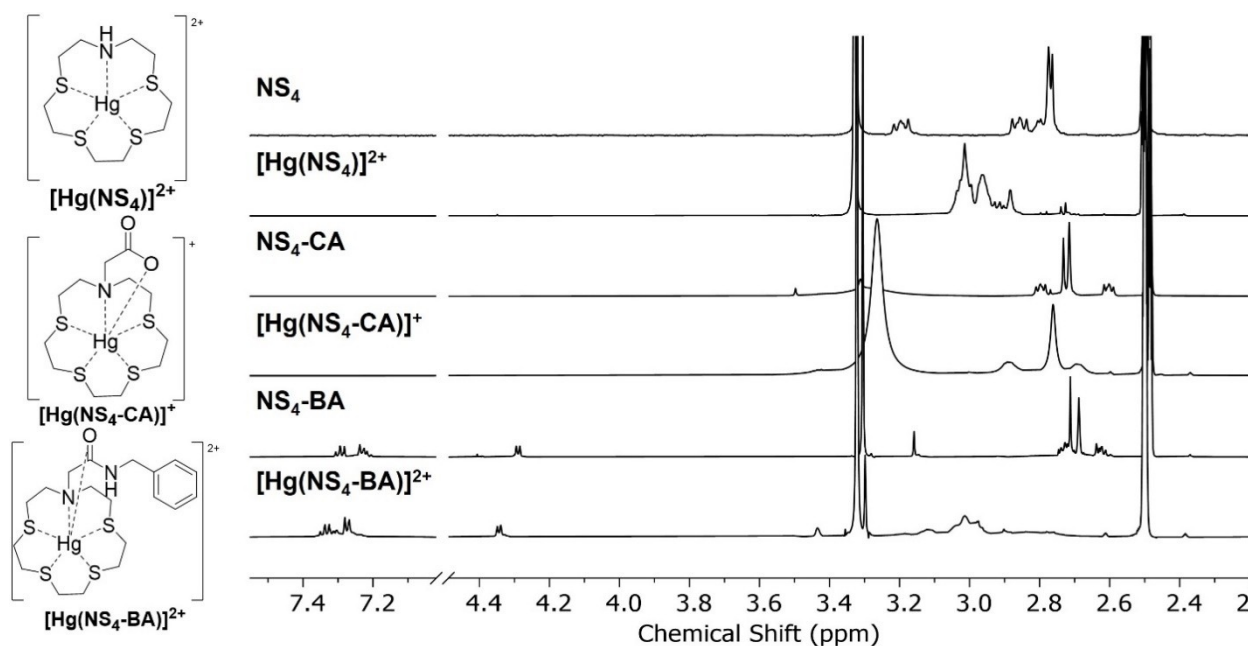


Figure 3. ^1H NMR spectra of NS_4 (5), $\text{NS}_4\text{-CA}$ (7), $\text{NS}_4\text{-BA}$ (9) and their Hg^{2+} complexes (10, 11, 12) (600 MHz, DMSO, 25 °C).

NMR timescale and/or the existence of different conformers. To further investigate this, variable temperature ^1H NMR spectra were collected (Figure S31). In the investigated temperature range (15–55 °C), broadening of the peaks of $[\text{Hg}(\text{NS}_4)]^{2+}$ (10) was observed with a decrease in temperature. This could be a result of the fluxionality in the ligand backbone that is progressively slowed down at lower temperatures. Thus, the spectral broadness is likely attributed to the non-symmetrical distribution of the backbone around the metallic center, as pointed out by DFT calculations (see below). For $\text{NS}_4\text{-BA}$, spectral changes can be observed in the aromatic region (~7.3 ppm) upon metal complexation (Figure 3). This suggests a possible participation of the benzyl moiety in Hg^{2+} coordination, in agreement with the DFT results (see below).

To further evaluate the potential of our chelating architecture, the complex formation equilibria of the NS_4 backbone with Hg^{2+} were investigated in an aqueous solution via variable pH- ^1H NMR at 25 °C and 0.1 M NaNO_3 . The marked spectral variations observed with respect to the free ligand indicate the complexation event throughout the investigated pH range (Figure 4; for comparative spectra of free ligand and complexes see Figure S32). Particularly, similar to the complex in DMSO (see above), all the protons of the macrocyclic scaffold became almost equivalent, giving rise to a broad multiplet, which suggests the formation of an NS_4 coordination sphere around Hg^{2+} . It is worth noting that no significant influence of the solvent was observed since the resonances are similarly arranged in the different solvents (water vs. DMSO). ^1H NMR titrations performed at different metal-to-ligand molar ratios demonstrated that only a 1:1 metal-to-ligand complex exists (Figure S33).

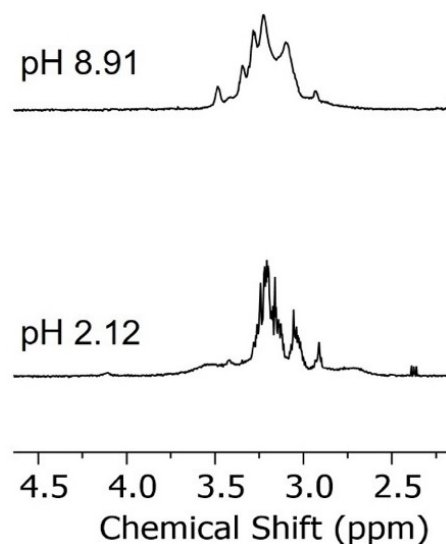


Figure 4. ^1H NMR spectra of $\text{Hg}^{2+}\text{-NS}_4$ (600 MHz, 25 °C, 90% H_2O + 10% D_2O , $C_{\text{Hg}^{2+}} = C_{\text{NS}_4} = 1 \cdot 10^{-3}$ M, $I = 0.15$ M NaNO_3) at different pH.

Since the $\text{Hg}^{2+}\text{-NS}_4$ complex was already formed at the lowest investigated pH (Figure 4 and S32), it was not possible to determine the exact values for the stability constant of the $\text{Hg}^{2+}\text{-NS}_4$ complex and only the minimum $\log\beta$ was computed to be 20.0 ± 0.5 . No further experiments to determine the exact value was attempted as generally the kinetic inertness is the key factor that dictates the *in vivo* integrity (see below) and these data are sufficient to suggest that the NS_4 scaffold afford a highly thermodynamically stable complex.

Density functional theory calculations

Despite numerous attempts, isolation of single-crystals of the $^{\text{nat}}\text{Hg}^{2+}$ -complexes suitable for X-ray measurements was unsuccessful. In the absence of these data, density functional theory (DFT) calculations were performed to elucidate the aqueous solution structure of the novel $\text{NS}_4\text{-CA}$ and $\text{NS}_4\text{-BA}$ complexes with Hg^{2+} . Only these two ligands were considered for the calculations as they better mimic the final electronic structure of a chelator bound to a tumour-targeting vector.

The 15-membered macrocycles synthesized in the present work are relatively low in symmetry compared to commonly employed macrocycles like DOTA, meaning that the only relevant stereochemical descriptor is the orientation of the five-membered chelate rings formed between the ethylene linkages of the backbone and the metal ion (λ/δ). By comparing all possible chelate geometries for $[\text{Hg}(\text{NS}_4\text{-CA})]^+$ (Table S1), it was determined that this complex adopts a single conformational isomer referred to as the lowest energy conformation of the carboxylic acid complex [conformer 9] in water wherein the metal center is coordinated by a five-membered pentagonal plane formed by the 5 heteroatoms of the backbone with a ($\delta, \delta, \delta, \lambda, \lambda$) configuration and capped by the sidearm carboxylic acid forming a 6-coordinated environment, as can be seen in Figure 5A. In this conformer, the ideal packing between all donor atoms is achieved as all the backbone sulfurs point downward (giving space to the carboxylic acid group to reach the cation without suffering steric strain or coulombic repulsion) relative to the sidearm such that a 6-membered distorted trigonal prismatic coordination environment can be established.

The lowest energy conformation of the carboxylic acid complex was determined to be 8.0 kJ/mol lower in energy than the following closest molecule. This demonstrated that only one stable arrangement exists for $[\text{Hg}(\text{NS}_4\text{-CA})]^{2+}$, thus ruling out the existence of different conformers in solution as the

thermal energy in solution at room temperature to 80 °C is 2.5–2.9 kJ/mol. Although no additional peaks were observed in the ^1H NMR spectrum of the complex, broadening within the peaks was recognizable (Figure 3). This can be therefore explained by the S–Hg interatomic distances ranging between 2.742 to 2.942 Å (Table S2), suggesting that there is unequal coordination with the backbone due to the asymmetry of the coordination environment. This can also be seen in the electrostatic potential maps shown in Figure 6A and 6B. As all the protons are no longer in the same chemical environment due to the asymmetric configuration $\delta, \delta, \delta, \lambda, \lambda$, upon coordination, precise splitting and resolution are no longer observed in the ^1H NMR spectra.

Following an identical computational approach, all relevant conformers of $[\text{Hg}(\text{NS}_4\text{-BA})]^{2+}$ were constructed and optimized (Table S3). These calculations show that the ($\lambda, \delta, \delta, \lambda, \lambda$) backbone arrangement with the simultaneous interaction of all the donor atoms in the scaffold and the chelation from both the benzyl amide sidearm carbonyl and η^6 benzene groups is the single most stable conformer in solution, referred to as lowest energy conformation of the benzyl amide complex [conformer 9], 17.3 kJ/mol lower in energy than the next nearest configuration. Both structures were examined in this study, namely the conformer that has $\pi\text{-Hg}^{2+}$ interaction (Figure 5B) and the one without (Figure 5C). The conformer with $\pi\text{-Hg}^{2+}$ chelation was ubiquitously lower in energy than the conformer without. This may be due to Hg's preferences for both soft π interactions and six-coordinate structures, which are both satisfied in the conformer with $\pi\text{-Hg}^{2+}$ interaction (Figure 5B), as opposed to the structure without (Figure 5C).

As can be seen in Table S4, the η^6 benzene– Hg^{2+} distance (from the center of the plane of the benzene ring) is 4.186 Å, significantly longer than typical coordination lengths, as π -cation interactions for Hg^{2+} have been observed in the range of 3.5–4.5 Å and have been seen generally for cations in protein

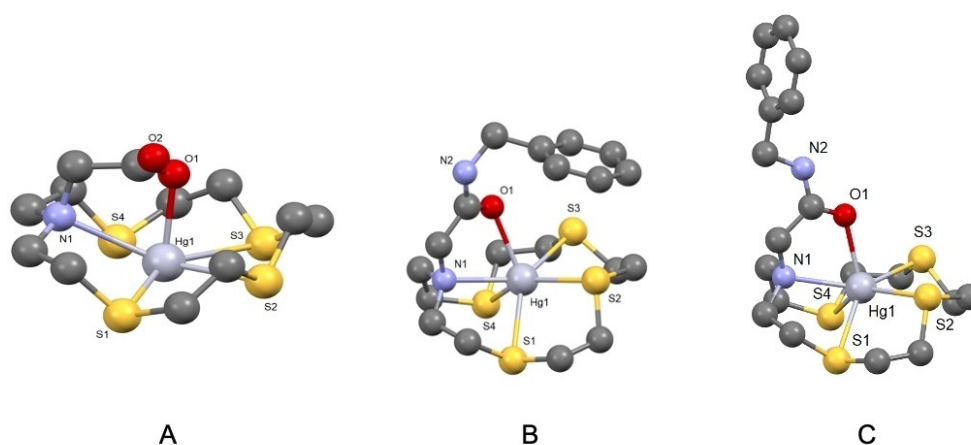


Figure 5. A) Lowest energy B3LYP/6-311G**/SDD/PCM optimized geometry of $[\text{Hg}(\text{NS}_4\text{-CA})]^+$ complex. B3LYP/6-311G**/SDD/PCM optimized geometries of the Hg complex of the $\text{NS}_4\text{-BA}$ ligand with B) and without C) π -cation interaction. The structures are visualized with the Mercury software package.^[40] Hydrogens were omitted for clarity.

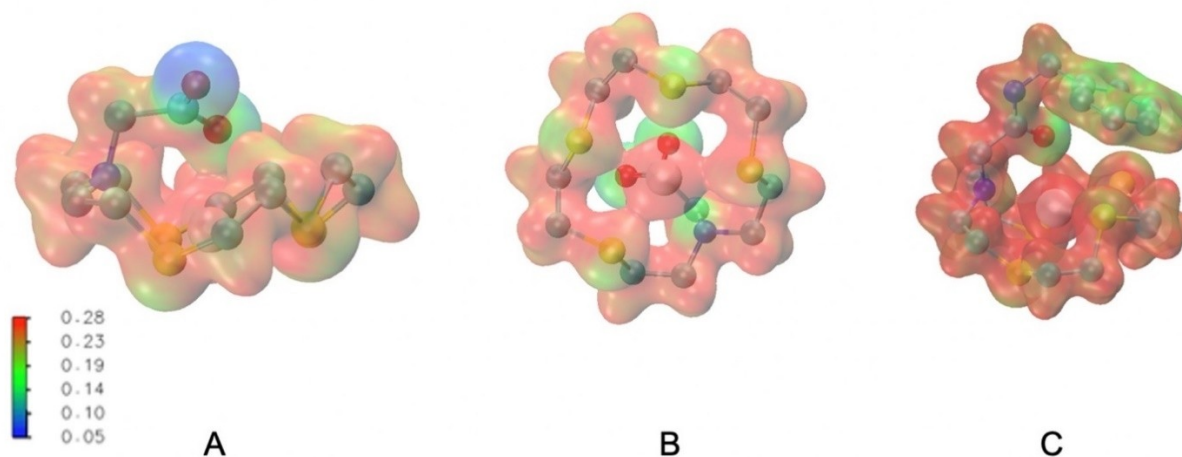


Figure 6. Isodensity surfaces colour-coded with electrostatic potential for the lowest energy conformer of $[\text{Hg}(\text{NS}_4\text{-CA})]^+$ (A: side view, B: bottom view) and C: $[\text{Hg}(\text{NS}_4\text{-BA})]^{2+}$ generated by MultiFWN.^[41,42] The scale is arbitrary, where red indicates a relative positive charge and blue represents a relative negative charge.

coordination systems as far away as 6 \AA .^[43,44] Regardless, to demonstrate the presence of a “real” $\pi\text{-Hg}^{2+}$ interaction, the Gibbs free energies in solution were obtained for this structure with and without the participation of the benzyl group while maintaining the backbone and carbonyl coordination identical, as can be seen in Figure 5C. The energy of the structure with benzyl coordination (Figure 5B) is 37.9 kJ/mol lower than that of the uncoordinated benzene structure, underscoring the massive role that the $\pi\text{-cation}$ interaction plays in stabilizing the coordination environment of the $[\text{Hg}(\text{NS}_4\text{-BA})]^{2+}$ complex.

To further understand why the lowest energy conformation of the benzyl amide complex (conformer 9) possesses the lowest energy, a comparison to another optimized structure is useful. In conformer 5 that has a backbone arrangement of

$(\lambda, \delta, \delta, \lambda, \lambda)$, the backbone and the sidearm behave very similarly to the lowest energy conformation in terms of chelation geometries, packing motifs and interatomic distances (Tables S4 and S5). The most stable conformers 5 ($\Delta G = 18.6 \text{ kJ/mol}$) (Figure 7A) and 9 ($\Delta G = 0.0 \text{ kJ/mol}$) (Figure 7B) were able to achieve the most efficient packing of the coordinating elements while minimizing the steric strain on the chelate complex, where one or both sidearm-adjacent sulfurs (S1 and S4) are pointing away from the pendant arm, thus allowing for much more effective carbonyl coordination and are consequently more stable. Whereas, in structures where S1 and S4 were pointing upwards towards the sidearm (i.e., $\Delta G_{\text{conformer 2}} = 45.0 \text{ kJ/mol}$ and $\Delta G_{\text{conformer 3}} = 52.4 \text{ kJ/mol}$), the electrostatic and steric repulsion

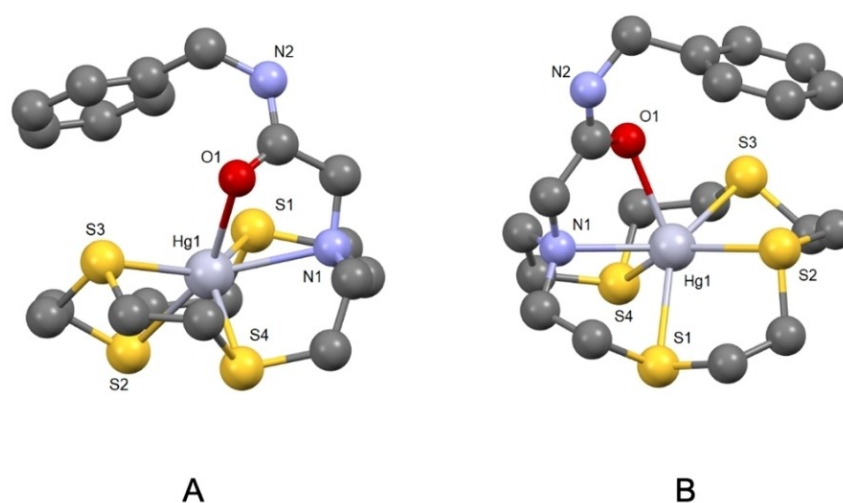


Figure 7. B3LYP/6-311G**/SDD optimized geometry of the conformer 5 $(\lambda, \delta, \delta, \lambda, \lambda)$ (A) and lowest energy conformer of the benzyl amide complex [conformer 9] (B) of $[\text{Hg}(\text{NS}_4\text{-BA})]^{2+}$ visualized with the Mercury software package.^[40] Hydrogens were omitted for clarity.

of these groups pushes away the carbonyl group and limits its participation in the coordination.

Despite the similarities of conformers 5, the lowest energy conformation of the benzyl amide complex (conformer 9) is 18.6 kJ/mol lower in energy. The most significant differences between these two structures lie in the coordination behaviour of the side arm. Conformer 5 shows much tighter packing of the benzyl amide carbonyl group (conformer 5: 2.466 Å, lowest energy conformation of the benzyl amide complex [conformer 9]: 2.658 Å), whereas the mercury ion in the lowest energy conformation of the benzyl amide complex is much closer to the benzene group (conformer 5: 4.724 Å, conformer 9: 4.186 Å). Conformer 5 is significantly higher in energy than the lowest energy conformation of the benzyl amide complex, despite the relatively long benzene-Hg coordination length: this suggests that the π -cation interaction driving the stabilization of the complex is much less distance-dependent than that of carbonyl coordination.

$[^{197m}\text{gHg}]\text{Hg}^{2+}$ radiolabeling studies

$[^{197m}\text{gHg}]\text{Hg}^{2+}$ concentration-dependent radiolabeling experiments with the novel sulfur-rich derivatives (NS₄, NS₄-CA, and NS₄-BA) were conducted using a newly developed iTLC protocol to determine the radiochemical yield (RCY%) (see Supporting Information). DOTA was tested alongside our macrocycles for comparison purposes to assess and further demonstrate the key role of sulfur in Hg²⁺ binding. The labelling conditions for the concentration-dependent labelling were chosen by screening the effect of different reaction times and temperatures on the RCYs (Table S6-S8); based on the obtained results, 1 h incubation time and pH 7 were used (Figure 8).

As shown in Figure 8, at 80 °C after 1 h, quantitative $[^{197m}\text{gHg}]\text{Hg}^{2+}$ incorporation was obtained with both NS₄ and NS₄-BA at 10⁻⁴ M. Decreasing the ligand concentration to 10⁻⁵ and 10⁻⁶ M afforded RCYs equal to 96.0 ± 0.3% and 31.3 ± 2.0%,

respectively, for NS₄-BA. RCYs for NS₄ under the same conditions were 83.7 ± 2.7% and 44.3 ± 0.8%, respectively. Unexpectedly, for NS₄-CA, the RCY was already relatively low (72.8 ± 2.8%) at 10⁻³ M, so the effect of the further decrease in ligand concentration on the radiometal incorporation was not assessed. Contrarily, at 80 °C, the RCYs of the commercial ligand DOTA (10⁻³ M) were drastically lower (<5%), even after prolonged reaction times (>1 h). These results demonstrate that the insertion of sulfur donor atoms in our ligands has increased the affinity to $[^{197m}\text{gHg}]\text{Hg}^{2+}$.

When the labelling temperature was lowered to 37 °C, while keeping all the other reaction conditions constant, the RCYs for NS₄-BA at concentrations from 10⁻⁴ M to 10⁻⁶ M were 93.2 ± 3.2%, 33.8 ± 2.1% and 0.0 ± 0.0%, respectively. RCYs for NS₄ under the same conditions were 87.3 ± 2.3% (10⁻³ M), 83.5 ± 2.9% (10⁻⁴ M), 9.7 ± 3.2% (10⁻⁵ M) and 0.0 ± 0.0% (10⁻⁶ M), respectively. For NS₄-CA, at 10⁻³ M, the RCY was 32.9 ± 4.3% (lower concentrations were not tested for the same reasons outlined above). Under the same reaction conditions, the $[^{197m}\text{gHg}]\text{Hg}$ -labelling yields of the NS₄-CA derivative were markedly lower in comparison to NS₄ and NS₄-BA. This could be attributed to its hard carboxylic anion being poorly compatible with the soft $[^{197m}\text{gHg}]\text{Hg}^{2+}$ ion. The synthesis the NS₄-CA analogue where the COOH group is converted to the equivalent borderline amide handle could be useful in testing this assumption.

Overall, a general trend is observed: with a decrease in temperature, the RCYs decreased and longer reaction times were required. This is likely attributable to the macrocyclic structure of the chelators. Indeed, as widely reported in the literature, due to their structural rigidity, their reaction kinetics are often slow, so relatively harsh complexation conditions are commonly required.^[1] Despite this, the advantage of choosing a macrocyclic structure is related to the high in vivo integrity of the resulting complex resulting from their more fixed geometry.^[45]

It should be noted that the labeling of these sulfur-rich chelators was also tested with a variety of medically relevant

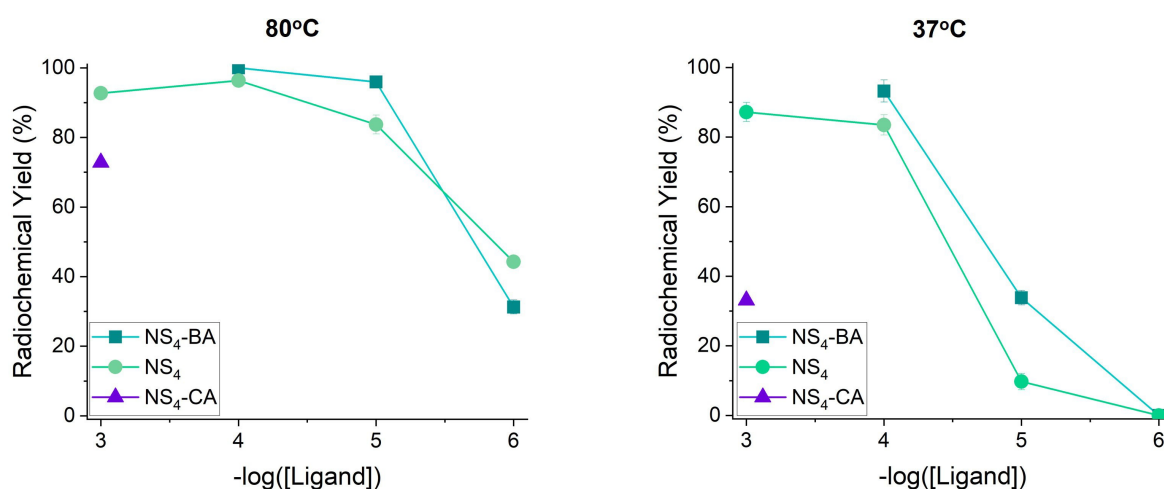


Figure 8. $[^{197m}\text{gHg}]\text{HgCl}_2$ radiochemical yields (RCYs) at various ligand concentrations for NS₄ (5), NS₄-CA (7), and NS₄-BA (9) (1 M NH₄OAc, pH 7), at 80 °C (left) and 37 °C (1 h reaction time, $n=3$) (right).

radioisotopes such as $[^{64}\text{Cu}]\text{Cu}^{2+}$, $[^{213}\text{Bi}]\text{Bi}^{2+}$, $[^{111}\text{In}]\text{In}^{3+}$ and $[^{203/212}\text{Pb}]\text{Pb}^{2+}$. In these cases, no radiometal incorporation was observed, agreeing with the data reported by Chen et al. and further demonstrating that these chelators are highly selective to Hg^{2+} compared to other metals.^[34]

Kinetic inertness of $[^{197\text{m/g}}\text{Hg}][\text{Hg}(\text{NS}_4\text{-BA})]^{2+}$

The results obtained in the labeling studies demonstrated that $\text{NS}_4\text{-BA}$ possessed the highest $[^{197\text{m/g}}\text{Hg}]\text{Hg}^{2+}$ incorporation yields among the investigated ligands. Prompted by this encouraging result, *in vitro* assays were conducted to assess the integrity of the $[^{197\text{m/g}}\text{Hg}][\text{Hg}(\text{NS}_4\text{-BA})]^{2+}$ complex in biologically relevant media and predict its suitability for future *in vivo* studies.

The inertness of the $[^{197\text{m/g}}\text{Hg}][\text{Hg}(\text{NS}_4\text{-BA})]^{2+}$ complex was studied through competition assays against glutathione (GSH) and human serum. GSH was chosen as it is the most abundant non-protein thiol present in mammalian cells (millimolar concentrations) where it serves as an intracellular antioxidant regulating cellular redox states.^[46] This small molecule is known to have a high affinity for soft cations such as Hg^{2+} , allowing it to be an excellent competitor for our chelators. On the other hand, human serum is a standard media used in competition assays to gain insight into the complex behavior within the human body.^[47,48]

To the radiometal complex, GSH (50 mM) was added such that the final GSH concentration mimicked *in vivo* conditions within cells (2.12 mM).^[46] Over 3 days, GSH was incubated with $[^{197\text{m/g}}\text{Hg}][\text{Hg}(\text{NS}_4\text{-BA})]^{2+}$ complex at 37 °C. At 10 h and 3 d, aliquots were removed and analyzed by iTLC; the percent intact complex was determined to be $97.2 \pm 0.3\%$ and $92.8 \pm 0.5\%$, respectively, as reported in Table S9. This overall stability of $[^{197\text{m/g}}\text{Hg}][\text{Hg}(\text{NS}_4\text{-BA})]^{2+}$ against GSH over 3 days indicates the formation of a highly kinetically inert complex, providing insight into how the stability might compare within cells.

Several protocols were tested in order to determine the human serum integrity of the $[^{197\text{m/g}}\text{Hg}]\text{Hg}^{2+}$ -complexes as described in the Supporting Information. However, sodium dodecyl sulfate–polyacrylamide gel electrophoresis (SDS-PAGE) was the only method that produced accurate and reproducible results. As shown in Figure S35, the electrophoretic migration of unchelated $[^{197\text{m/g}}\text{Hg}]\text{Hg}^{2+}$ in human serum, $[^{197\text{m/g}}\text{Hg}]\text{Hg}^{2+}$ complex in PBS (control) and $[^{197\text{m/g}}\text{Hg}]\text{Hg}^{2+}$ complex in human serum are different. From the integration of the signals, it was, therefore, possible to obtain the percentages of the intact $[^{197\text{m/g}}\text{Hg}]\text{Hg}^{2+}$ complex over time. Using this method, the kinetic inertness of the radiolabeled NS_4 and $\text{NS}_4\text{-BA}$ complexes was tested against human serum over 24 h at 37 °C. NS_4 was included in this study to explore the effect of the added amidic side arm of $\text{NS}_4\text{-BA}$ on the integrity of the resulting complex under biologically relevant conditions.

As shown in Figure 9, the percent intact complex in human serum was determined at 2 h and 24 h to be $71.5 \pm 7.5\%$ and $59.8 \pm 10.9\%$, $84.7 \pm 3.4\%$ and $74.1 \pm 7.0\%$ for $[^{197\text{m/g}}\text{Hg}][\text{Hg}(\text{NS}_4)]^{2+}$ and $[^{197\text{m/g}}\text{Hg}][\text{Hg}(\text{NS}_4\text{-BA})]^{2+}$, respectively. These results

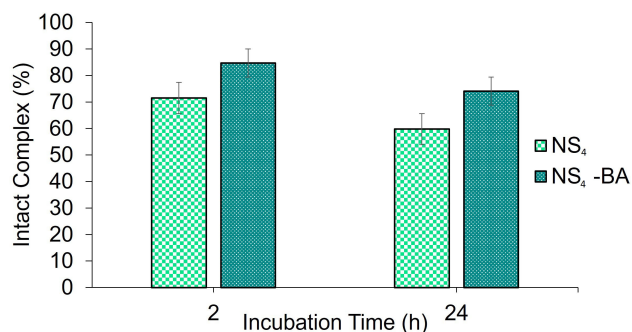


Figure 9. Human serum integrity of $[^{197\text{m/g}}\text{Hg}][\text{Hg}(\text{NS}_4)]^{2+}$ and $[^{197\text{m/g}}\text{Hg}][\text{Hg}(\text{NS}_4\text{-BA})]^{2+}$ at 37 °C ($n = 3$).

indicate that the $\text{NS}_4\text{-BA}$ complex is significantly more kinetically inert in human serum compared to the NS_4 macrocycle alone, in agreement with the DFT calculations that suggest the carbonyl and π -electron interactions induce an increase in the overall complex stability. The drop in the % of intact $[^{197\text{m/g}}\text{Hg}]\text{Hg}^{2+}$ complex over 22 h is likely related to the presence of biologically relevant substrates (most likely sulfur-rich proteins) that compete and displace the chelator-bound metal ion.

The high kinetic inertness demonstrated by $[^{197\text{m/g}}\text{Hg}][\text{Hg}(\text{NS}_4\text{-BA})]^{2+}$ suggests this compound to be a viable candidate for $^{197\text{m/g}}\text{Hg}$ -based radiopharmaceuticals.

Conclusion

This work demonstrated the advantages of incorporating sulfur donors within a chelate construct to afford the first-reported stable and kinetically inert $[^{197\text{m/g}}\text{Hg}]\text{Hg}^{2+}$ complexes. The macrocyclic scaffold (NS_4) and its bifunctional analogues ($\text{NS}_4\text{-CA}$, and $\text{NS}_4\text{-BA}$) were synthesized via a 5, 7, and 9-step process, respectively. Non-radioactive Hg^{2+} complexes were prepared and characterized. According to NMR and DFT calculations, the $[\text{Hg}(\text{NS}_4)]^{2+}$ complex entails the coordination of the NS_4 array of atoms forming a thermodynamically stable complex. In $[\text{Hg}(\text{NS}_4\text{-CA})]^{2+}$, the coordination of the carboxylic pendant arm in a 6-coordinated distorted trigonal prismatic environment was demonstrated, while Hg^{2+} coordinated to all the donor atoms within the $\text{NS}_4\text{-BA}$ ligand backbone as well as to the carbonyl and the π -electrons from the benzyl group.

Labeling experiments with $[^{197\text{m/g}}\text{Hg}]\text{Hg}^{2+}$ demonstrated that the novel thiocrown derivatives possessed significantly increased radiometal binding ability compared to the commercial ligand DOTA due to the presence of soft sulfur donor atoms that are optimal for Hg^{2+} coordination.

The $\text{NS}_4\text{-BA}$ ligand afforded a kinetically inert $[^{197\text{m/g}}\text{Hg}]\text{Hg}^{2+}$ complex against competitors such as endogenous serum proteins and GSH over 24 h and 3 days, respectively. In comparison, when $[^{197\text{m/g}}\text{Hg}]\text{Hg}^{2+}$ was bound to NS_4 , a decreased kinetic inertness of the complex was detected. These results were rationalized by DFT studies, which demonstrated

the role of the π -cation interaction between the metal centre and benzyl group in the formation of a stable chelation environment for the $[\text{Hg}(\text{NS}_4\text{-BA})]^{2+}$ complex.

This study provides essential information on the chelating systems that can be incorporated into $^{197\text{m/g}}\text{Hg}$ radiopharmaceuticals, allowing further development of this theranostic pair. To the best of our knowledge, this is the first example of a chelator capable of yielding high radiomercury incorporation in a stable complex under biocompatible conditions (pH 7 and 37°C), enabling the future use of a plethora of targeting vectors including temperature-sensitive biomolecules (i.e. antibodies).^[25,49–51] As a result, the syntheses of bifunctional $\text{NS}_4\text{-BA}$ and resulting bioconjugates are currently underway, with in vivo biodistribution and imaging studies planned in due course.

Experimental Section

Materials and methods: All solvents and reagents were purchased from commercial suppliers and used as received unless otherwise noted. Ultrapure concentrated hydrochloric acid (HCl, 99.99% trace metal grade, 37%), sodium hydroxide (NaOH, ACS reagent, $\geq 97\%$, pellets), sodium deuterioxide (NaOD, 30 wt% in D_2O), deuterium chloride (DCI, 35 wt% in D_2O), dimethyl sulfoxide (DMSO), DOTA, and human serum were purchased from Sigma Aldrich (St. Louis, MO). Millipore system (Direct-Q® 3UV with Pump, $18\text{ M}\Omega\text{ cm}^{-1}$) provided ultrapure water. Deuterated solvents used for NMR analysis were purchased from Sigma or Cambridge isotope laboratories Inc and exhibited an isotopic purity between 99.9% and 99.8%. Solvents noted as “dry” were obtained following storage over 3 Å molecular sieves under an argon environment. Flash column chromatography was generally employed and was carried out using silica gel 60 (0.040–0.630 mm) using a stepwise solvent polarity gradient correlated with TLC mobility. Chromatography solvents used were ether, toluene, hexane, ethyl acetate, acetone, dichloromethane, methanol (Sigma Aldrich). Mercury(II) nitrate solution ($C_{(\text{Hg}(\text{NO}_3)_2)} = 0.05\text{ mol/L}$, in 0.1 M HNO_3 , Titripur®, Sigma Aldrich) was used for NMR titrations.

^1H and ^{13}C NMR spectra were recorded either on a Bruker AVANCE III 600 MHz QCI cryoprobe, Bruker AVANCE III 500 MHz, or Bruker AVANCE III 400 MHz instruments. Chemical shifts are reported in parts per million (ppm) and are referred to the residual solvent peak. Multiplicity is reported as follows: s=singlet, t=triplet, m=multiplet and br=broad peak. The coupling constants (J) are reported in hertz (Hz). Low-resolution mass spectrometry (ESI-LRMS) was performed using an Advion expression CMS spectrometer with an ESI electrospray ionization source, which was run using Advion Mass Express software. High-resolution electrospray-ionization mass spectrometry (ESI-HRMS) was performed on an Agilent 6210 time-of-flight instrument (TOF). The radiolabeling of ligands was monitored using silica-impregnated instant thin-layer chromatography paper (iTLC-SG, Agilent Technologies, Santa Clara, CA, USA) and analysed on an Eckert & Ziegler AR-2000 TLC scanner and processed with Eckert & Ziegler WinScan software (Hopkinton, USA). A Capintec CRC 15R dose calibrator well counter set at the $^{197\text{m/g}}\text{Hg}$ calibration was used to measure the activity prior to radiolabeling reactions. Bio-rad Mini-PROTEAN Tetra Vertical Electrophoresis Cell instrument was used for all sodium dodecyl sulfate–polyacrylamide gel electrophoresis (SDS-PAGE) measurements with 4–20% Mini-PROTEAN® TGX™ Precast Protein Gels. The SDS-PAGE gel electrophoresis reagents, including the MW stand-

ards, TGS buffer, Laemmli sample buffer, and Bio-Safe™ Coomassie stain, were all also purchased from Bio-rad.

Caution!!! $^{197\text{m/g}}\text{Hg}$ produces ionizing radiation and should be handled in laboratories approved for radioactive work using safe lab practices.

Caution!!! Mercury is a toxic heavy metal, and its compounds should be treated accordingly.

Synthesis of NS_4 and derivatives: The NS_4 macrocyclic synthesis was accomplished through a combination and modification of two procedures.^[35,38]

***N*-tert-nutoxycarbonyl bis(2-chloroethyl)amine (1):** To a suspension of bis(2-chloroethyl)amine hydrochloride (6.00 g, 33.6 mmol, 1 equiv.) in CH_2Cl_2 (72 mL) and 10% aqueous sodium hydroxide (36 mL) was added a solution of di-*tert*-butyl dicarbonate (7.32 g, 33.6 mmol, 1 equiv.) in CH_2Cl_2 (36 mL). The reaction mixture was stirred for 23 h at room temperature, diluted with CH_2Cl_2 (6 mL) and water (6 mL), and the two phases were separated. The aqueous layer was extracted with CH_2Cl_2 ($3 \times 12\text{ mL}$) and the combined organic layers were dried over Na_2SO_4 , filtered and the solvent was removed under reduced pressure to give **1** (8.01 g, 33.1 mmol, 1 equiv., yield 98%) as a colourless oil. $R_f = 0.32$ (hexane – ethyl acetate (EtOAc) 7:3); ^1H NMR (CDCl_3 , 400 MHz): δ 3.72–3.58 (8H, m, $\text{NCH}_2 + \text{CH}_2\text{Cl}$), 1.50 (9H, s, $\text{C}(\text{CH}_3)_3$); ^{13}C NMR (CDCl_3 , 100 MHz, the asterisk denotes the signals of the rotamer): δ 154.9 (C=O), 80.7 ($\text{C}(\text{CH}_3)_3$), 51.0, 50.8* (NCH_2), 42.1, 41.9* (CH_2Cl), 28.3 ($\text{C}(\text{CH}_3)_3$). The MS data was not obtained, as the Boc protecting group is fragmented in the mass spectrometer and the bis(2-chloroethyl)amine mass was not observed in the mass. TLC was used to monitor the reaction.

2,2-((Azanediylbis(ethane-2,1-diyl))bis(sulfanediyl))bis(ethan-1-ol) (2): To a suspension of **1** (5.96 g, 24.6 mmol, 1 equiv.) in dry dimethyl formamide (18 mL) 2-mercaptoethanol (4.3 mL, 61.5 mmol, 2.5 equiv.) and K_2CO_3 (8.50 g, 61.5 mmol, 2.5 equiv.) were added. The reaction mixture was stirred for 69 h at 40°C under nitrogen. The solvent was removed under reduced pressure and the remainder was diluted with EtOAc (6 mL) and water (6 mL). The aqueous layer was extracted with EtOAc ($6 \times 12\text{ mL}$) and the combined organic layers were dried over Na_2SO_4 that was filtered afterwards. The solvent was removed under reduced pressure to give **2** (8.01 g, 24.6 mmol, 1 equiv., assuming 100% yield as the product was carried onto the next step without further purification) as a colourless oil. $R_f = 0.28$ (100% ether); ^1H NMR (MeOD, 400 MHz): δ 3.69 (4H, t, J 6.7, CH_2OH), 3.42 (4H, m, NCH_2), 2.75–2.62 (8H, m, SCH_2 , CH_2S), 1.47 (9H, s, $\text{C}(\text{CH}_3)_3$); ^{13}C NMR (MeOD, 100 MHz, the asterisk denotes the signals of the rotamer): δ 157.1 (C=O), 81.5 ($\text{C}(\text{CH}_3)_3$), 62.6 (CH_2OH), 35.4 (NCH_2), 31.7, 31.1* (SCH_2), 28.7 ($\text{C}(\text{CH}_3)_3$); ESI-HRMS m/z calcd. for $[\text{C}_{13}\text{H}_{27}\text{NO}_4\text{S}_2 - \text{C}_5\text{H}_7\text{O}_2]^+$ 226.09355; found 226.087 [M-Boc] $^+$.

***Tert*-butyl bis(2-((2-chloroethyl)thio)ethyl)carbamate (3):** To a stirred solution of **2** (8.01 g, 24.6 mmol, 1 equiv.) in dry CH_2Cl_2 (400 mL) under argon, triethylamine (20.5 mL, 148 mmol, 6 equiv.) and tosyl chloride (23.1 g, 121 mmol, 4.9 equiv.) were added. The reaction mixture was stirred for 22 h at room temperature. The reaction mixture was diluted with CH_2Cl_2 (10 mL), washed with water ($2 \times 20\text{ mL}$) and brine (10 mL). The organic layer was dried over Na_2SO_4 . The resulting organic layer was filtered, and the solvent was removed under reduced pressure. Flash chromatography of the resulting residue (toluene, toluene-EtOAc 9:1 gradient then hexane-ether 4:1) gave **3** (3.31 g, 9.15 mmol, 1 equiv., yield 60% for two steps) as a pale-yellow oil. $R_f = 0.29$ (100% toluene); ^1H NMR (CDCl_3 , 400 MHz): δ 3.64 (4H, t, J 7.8, CH_2Cl), 3.43–3.35 (4H, m, NCH_2), 2.93–2.84 (4H, m, SCH_2), 2.76–2.66 (4H, m, SCH_2), 1.48 (9H, s, $\text{C}(\text{CH}_3)_3$); ^{13}C NMR (CDCl_3 , 100 MHz, the asterisk denotes the

signals of the rotamer): δ 154.9 (C=O), 80.3 (C(CH₃)₃), 48.6, 48.2* (NCH₂), 43.1 (CH₂Cl), 34.3 (SCH₂), 30.9, 30.5* (SCH₂), 28.4 (C(CH₃)₃); ESI-HRMS *m/z* calcd. for [C₁₃H₂₅Cl₂NO₂S₂-C₅H₇O₂]⁺ 262.02577; found 262.0291 [M-Boc]⁺.

Tert-butyl 1,4,7,10-tetrathia-13-azacyclopentadecane-13-carboxylate (4): To a stirred solution of KI (23.5 mg, 0.140 mmol, 0.1 equiv.) and Cs₂CO₃ (1.02 g, 3.13 mmol, 2.2 equiv.) in dry, degassed dimethylformamide (DMF, 90 mL) under argon at 50 °C were added a solution of **3** (506 mg, 1.40 mmol, 1 equiv.) and 1,2-ethanedithiol (0.13 mL, 1.56 mmol, 1.1 equiv.) in dry DMF (10 mL) slowly over 48 h. The solvent was removed under reduced pressure and the resulting reaction mixture was diluted with EtOAc (6 mL) and water (6 mL). The aqueous layer was extracted using EtOAc (3 × 6 mL). The organic layers were washed with H₂O (6 mL), brine (6 mL) and dried over Na₂SO₄. The resulting organic layer was filtered, and the solvent was removed under reduced pressure. Flash chromatography of the resulting residue (hexane-ether 6:1) gave **4** (153 mg, 0.400 mmol, 1 equiv., yield 29%) as a white solid. *R*_f = 0.30 (hexane-ether 6:1); ¹H NMR (CDCl₃, 400 MHz): δ 3.44 (4H, d, *J* 7.3, NCH₂), 2.87–2.65 (16H, m, SCH₂), 1.47 (9H, s, C(CH₃)₃); ¹³C NMR (CDCl₃, 100 MHz, the asterisk denotes the signals of the rotamer): δ 154.94 (C=O), 80.27 (C(CH₃)₃), 49.35, 48.87* (NCH₂), 32.84, 32.63, 31.04, 30.75 (SCH₂), 28.41 (C(CH₃)₃); ESI-HRMS *m/z* calcd. for [C₁₅H₂₉NO₂S₄]⁺ 383.10812; found 383.400 [M]⁺.

1,4,7,10-Tetrathia-13-azacyclopentadecane chloride (5): A solution of **4** (153 mg, 0.400 mmol) in CH₃OH (1.66 mL) and EtOAc (3.3 mL) was stirred for 24 h at 45 °C. To the stirred solution, concentrated HCl (0.33 mL) was added drop wise. The solvent was removed under reduced pressure, giving **5** (107 mg, 0.380 mmol, 1 equiv., yield 94%) as a yellow solid. ¹H NMR (D₂O, 400 MHz): δ 3.48 (4H, t, *J* 6.4, NCH₂), 3.08–2.93 (16H, m, SCH₂); ¹³C NMR (D₂O, 100 MHz): δ 45.9 (NCH₂), 32.0, 31.9, 31.7, 27.8 (SCH₂); ESI-HRMS *m/z* calcd. for [C₁₀H₂₁NS₄H]⁺ 284.0635; found 284.0624 [M + H]⁺.

Tert-butyl 2-(1,4,7,10-tetrathia-13-azacyclopentadecan-13-yl)acetate (6): A stirred solution of **5** (50.3 mg, 0.160 mmol, 1 equiv.), K₂CO₃ (97.9 mg, 0.710 mmol, 4.4 equiv.), NaI (2.5 mg, 0.020 mmol, 0.1 equiv.) in dry acetonitrile (2 mL) was stirred at room temperature. To the stirred solution tert-butyl bromoacetate (20.8 μ L, 0.140 mmol, 0.9 equiv.) was added. The resulting solution was stirred for 24 h, filtered through celite and the solvent was removed under reduced pressure. Flash chromatography of the resulting residue (hexane-acetone 8:2) gave **6** (39.7 mg, 0.100 mmol, 1 equiv., yield 64%) as a white solid. *R*_f = 0.34 (hexane-EtOAc 9:1); ¹H NMR (CDCl₃, 400 MHz): δ 3.35 (2H, s, (CH₂)C=O), 3.00–2.60 (20H, m, SCH₂), 1.49 (9H, s, C(CH₃)₃); ¹³C NMR (CDCl₃, 100 MHz): δ 170.46 (C=O), 81.27 (C(CH₃)₃), 56.27 ((CH₂)C=O), 55.4 (NCH₂), 33.10, 32.61, 32.47, 31.16 (SCH₂), 28.20 (C(CH₃)₃); ESI-HRMS *m/z* calcd. for [C₁₆H₃₁NO₂S₄H]⁺ 398.13159; found 398.1201 [M + H]⁺.

2-(1,4,7,10-Tetrathia-13-azacyclopentadecan-13-yl)acetic acid (7): A solution of **6** (63.0 mg, 0.160 mmol) in trifluoroacetic acid (TFA, 2 mL) and CH₂Cl₂ (1.5 mL) was stirred for 4 h at room temperature. CH₃OH was added and removed under reduced pressure to displace the TFA. Flash chromatography of the resulting residue (CH₂Cl₂-CH₃OH gradient 100, 98:2, 95:5, 90:10) gave **7** (46.9 mg, 0.130 mmol, 1 equiv., yield 84%) as a white solid. *R*_f = 0.15 (CH₂Cl₂-CH₃OH 95:5); ¹H NMR (600 MHz, DMSO) δ 3.39 (2H, s, (CH₂)C=O), 2.86–2.81 (4H, m, NCH₂), 2.74 (4H, s, H_a), 2.73 (8H, s, H_b), 2.66–2.60 (4H, m, H_c); ¹³C NMR (151 MHz, DMSO) δ 172.77 (C=O)*, 55.55 (CH₂)C=O, 54.87(NCH₂), 32.33 (C_a), 31.91 (C_b), 31.89 (C_c), 29.36 (C_d). *found from the HMBC; ESI-HRMS *m/z* calcd. for [C₁₂H₂₃NO₂S₄ + H]⁺ 342.06899; found 342.0476 [M + H]⁺.

2,5-Dioxopyrrolidin-1-yl 2-(1,4,7,10-tetrathia-13-azacyclopentadecan-13-yl)acetate (8): To a stirred solution of **7** (10.1 mg, 0.0293 mmol, 1 equiv.) in dry DMF (2 mL), N-hydroxysuccinimide (3.4 mg, 0.030 mmol, 1 equiv.), 1-ethyl-3-(3-dimethylaminopropyl) carbodiimide (EDC, 7.36 mg, 0.0383 mmol, 1.3 equiv.) were added at room temperature under argon and left to react for 48 h. The reaction mixture was diluted with CH₂Cl₂ (6 mL), washed with a solution of H₂O (6 mL) and 15% NaHCO₃ (0.5 mL), then with H₂O (18 mL) three times, and brine (6 mL). The organic layer was dried over Na₂SO₄, filtered and solvent removed under reduced pressure to give **8** (10.9 mg, 0.0249 mmol, 1 equiv., yield 85%) as a yellow oil. *R*_f = 0.85 (CH₂Cl₂-CH₃OH 95:5); ¹H NMR (CDCl₃, 400 MHz): δ 3.80 (2H, s, (CH₂)C=O), 3.04–2.62 (24H, m, NCH₂ + SCH₂ + NC=O(CH₂)); ESI-LRMS *m/z* calcd. for [C₁₆H₂₆ N₂O₄S₄ + H]⁺ 439.1; found 439.1 [M + H]⁺.

N-benzyl-2-(1,4,7,10-tetrathia-13-azacyclopentadecan-13-yl)acetamide (9): To a stirred solution of **8** (10.9 mg, 0.0249 mmol), benzylamine (3.3 μ L, 0.0302 mmol) in dry CH₂Cl₂ (1 mL) *N,N*-diisopropylethylamine (DIPEA, 5.2 μ L, 0.0299 mmol) was added at 0 °C under argon. After addition, the solution was allowed to warm to room temperature and stirred for 24 h. The reaction mixture was diluted with CH₂Cl₂, washed with H₂O (3 × 6 mL) and brine (6 mL). The organic layer was dried with Na₂SO₄, filtered and the solvent removed under reduced pressure. Flash chromatography of the resulting residue (toluene-EtOAc 1:1) gave **9** (5.2 mg, 0.012 mmol, 1 equiv., yield 49%) as a yellow oil. *R*_f = 0.42 (toluene-EtOAc 1:1); ¹H NMR (CD₃CN, 500 MHz): δ 7.94 (1H, s, NH), 7.46–7.14 (5H, m, CH), 4.38 (2H, d, *J* 6.3, CH(CH₂)), 3.12 (2H, d, *J* 8.5, (CH₂)C=O), 2.82–2.50 (20H, m, NCH₂ + SCH₂); ¹³C NMR (CD₃CN, 150 MHz): δ 171.6 (C=O), 140.4, 129.4, 128.5, 128.0 (Ar-CH), 59.4 (C(C=O)), 55.9 (C(Ar-C)), 43.3 (NCH₂), 33.4, 32.9, 32.7, 30.6 (SCH₂); ESI-HRMS *m/z* calcd. for [C₁₉H₃₀N₂O₄S₄ + H]⁺ 431.13193; found 432.0869 [M + H]⁺.

Synthesis of non-radioactive Hg²⁺ complexes

[Hg(1,4,7,10-tetrathia-13-azacyclopentadecane)](Cl₂) (10): Compound **5** (8.0 mg, 0.028 mmol, 1 equiv.) was dissolved in ethanol (1.5 mL). To this colourless solution, a solution of HgCl₂ (9.6 mg, 0.035 mmol, 1.3 equiv.) in ethanol (1.5 mL) was added, and a white precipitate formed. The precipitate was isolated by centrifugation (14800 rpm, 2 min), the filtrate was decanted, and the solid was dried under vacuum to yield the product **10** as a white powdery solid (14.0 mg, 0.0289 mmol, 1 equiv., yield > 99%). ¹H NMR (DMSO, 600 MHz): δ : 3.05–2.82 (m, 20H, SCH₂ + NCH₂). ESI-HRMS *m/z* calcd. for C₁₀H₂₁HgNS₄²⁺ 242.5126; found 242.5118 [M]²⁺.

[Hg(2-(1,4,7,10-tetrathia-13-azacyclopentadecan-13-yl)acetic acid)](Cl₂) (11): Compound **7** (4.8 mg, 0.014 mmol, 1 equiv.) was dissolved in chloroform-ethanol (3:1) (0.8 mL). To this colourless solution, a solution of HgCl₂ (6 mg, 0.022 mmol, 1.6 equiv.) in ethanol (0.8 mL) was added, and a white precipitate formed. The precipitate was isolated by centrifugation (14800 rpm, 2 min), the filtrate was decanted, and the solid was dried under vacuum to yield the product **11** as a white powdery solid (9.4 mg 0.017 mmol, 1 equiv., yield, > 99%). ¹H NMR (DMSO, 600 MHz): δ : 3.47–3.40 (m, 2H, NC=O(CH₂)), 2.92–2.69 (m, 20H, NCH₂ + SCH₂). ESI-LRMS *m/z* calcd for C₁₂H₂₂HgNO₂S₄⁺ 542.0; found 542.1 [M]⁺.

[Hg(2-(N-benzyl-2-(1,4,7,10-tetrathia-13-azacyclopentadecan-13-yl)acetamide)](Cl₂) (12): Compound **9** (2.0 mg, 0.00464 mmol, 1 equiv.) was dissolved in ethanol-chloroform (3:1) (0.5 mL). To this colourless solution, a solution of HgNO₃ (2.4 mg, 0.0074 mmol, 1.6 equiv.) in ethanol (0.8 mL) was added, and a yellow precipitate formed. The precipitate was isolated by centrifugation (14800 rpm, 2 min), the filtrate was decanted, and the solid was dried under vacuum to yield the product **12** as a yellow powdery solid (1.3 mg,

0.020 mmol, 1 equiv., yield 50%). ^1H NMR (DMSO, 600 MHz): δ 7.35–7.32 (m, 2H, CH), 7.27 (d, J 7.2 Hz, 3H, CH), 4.34 (d, J 5.9 Hz, 2H, CH(CH₂)), 3.21–2.71 (m, 29H, (CH₂)C=O + NCH₂ + SCH₂)*. ESI-LRMS m/z calcd for [C₁₉H₃₀HgN₂OS₄²⁺ + NO₃⁻]⁺ 694.08256; found 694.9. [M + NO₃]⁺.

*Explained: Integration should be 22H. Exact integration was not obtained due to a combination of poor shimming of the sample, the low concentration of the sample and the peak attaining a broad shape.

NMR titrations: Variable pH ^1H NMR spectra of NS₄ (5) and its Hg²⁺ complex (10) were collected at 25 °C using a Bruker AVANCE II 600 MHz QCI cryoprobe spectrometer to investigate the acid-base properties of the former and the thermodynamic stability of the latter. The stock ligand solutions were prepared in H₂O + 10% D₂O at ligand concentration ranging from 0.5–2·10⁻³ M. Hg(NO₃)₂ was added at equimolar metal-to-ligand ratio. The ionic strength was adjusted using 0.1 M NaNO₃. Proper addition of HNO₃ or NaOH in H₂O was performed to set the pH. The stoichiometry of the Hg²⁺-NS₄ complex was assessed by adding different aliquots of Hg(NO₃)₂ to the NS₄ solution at pH 8 to obtain a metal-to-ligand ratio varying from 0:1 to 4:1. Water signal was suppressed using excitation sculpting suppression pulse scheme.^[52] All data were collected using standard Bruker parameters and processed with MestReNova 14.1.2-25024 software. The acidity constant of NS₄ (pK_a) and the minimum value of the stability constant of its Hg²⁺ complex (logβ) were refined using HypNMR software. All the equilibrium constants are referred to the $p\text{Hg}^{2+} + q\text{H}^+ + r\text{L}^- = \text{Hg}_p\text{H}_q\text{L}_r^{pm+q-r}$ where L represent NS₄ and are defined as cumulative formation constants (logβ_{par} = [Hg^pL^qH^r]/[Hg]^p[L]^q[H]^r). The formation constants of the hydroxo-Hg²⁺ species, taken from the literature data, were considered for the data treatment.^[53]

Density functional theory calculations: DFT calculations were performed using the Gaussian 16 software for all geometry optimizations, frequency analysis, and thermodynamic data that was extracted.^[54] Calculations were performed with the Becke three parameter, Lee-Yang-Parr (B3LYP) functional with the triple- ζ 6-311G** basis set for all the main group elements in the novel sulfur backbone derivatives (H, C, N, O, S) and were corrected with Grimme's dispersion correction along with Becke-Johnson damping (D3-BJ).^[55–58] The Stuttgart Dresden (SDD) small-core effective core potential (ECP) along with the respective SDD basis was used for Hg to include scalar relativistic effects.^[59] Structures were optimized in water using the polarizable continuum model (PCM). All conformers were created by constructing all possible stereochemically unique backbone/sidearm combinations manually and optimizing them at the Molecular Mechanics (MM) level using the Avogadro software.^[60] Structures were then re-optimized at higher level of theory until all possible chemically reasonable structures were obtained. Vibrational frequency calculations were performed at the optimized geometries to ensure true minima were obtained and to obtain solvated thermochemistry data. The Gibbs free energy of solvation was used to estimate the aqueous stability of each conformer in solution using the gas phase Gibbs energy and the Gibbs energy of solvation (Eq. (1)):

$$G_{\text{soln}} = G_{\text{gas}} + \Delta G_{\text{solv}} \quad (1)$$

These energies were calculated using zero-point energies scaled by 0.967, the corresponding scaling factor for B3LYP-6-311G** calculations.^[61] Geometry optimizations were performed without imposing any symmetric constraints.

Production of mercury-197m/g: Production of $^{197\text{m/g}}\text{Hg}$ was achieved through proton irradiation of gold targets via the $^{197}\text{Au}(p,n)^{197\text{m/g}}\text{Hg}$ nuclear reaction at the TR13 (13 MeV) cyclotron at

TRIUMF – Canada's particle accelerator center. $^{197}\text{Au}/^{197\text{m/g}}\text{Hg}$ separation and purification were accomplished via previously published procedures.^[62] Briefly, the Au target was dissolved in *aqua regia*, the solution was then loaded on to a prepared column of LN resin. The [$^{197\text{m/g}}\text{Hg}$]Hg²⁺ was eluted in 4 mL 6 M HCl while the ^{197}Au was retained on the resin. The $^{197\text{m/g}}\text{Hg}$ solution matrix was then exchanged to a 0.1 M HCl solution by multiple steps of evaporation and reconstruction. The final activity ranged from 90 to 140 MBq of [$^{197\text{m/g}}\text{Hg}$]Hg²⁺ obtained as HgCl₂ in 250–350 μL 0.1 M HCl. The radionuclidic purity of the obtained $^{197\text{m/g}}\text{Hg}$ was evaluated using γ -ray spectroscopy on an N-type co-axial high-purity germanium (HPGe) gamma spectrometer (CANBERRA, Mirion Technologies, Inc., San Ramon, CA, USA), calibrated with a 20 mL ^{152}Eu and ^{133}Ba source. Samples were prepared by mixing aliquots of $^{197\text{m/g}}\text{Hg}$ activity (1.2 MBq) with deionized water in a 20 mL glass vial to make a 20 mL sample and measured at a distance of 150 mm from the detector for 10 minutes, ensuring dead times below < 10%. Spectra were analysed using Genie-2000 software, using the 133.98 keV ($I_\gamma = 33.5\%$) and 164.97 keV ($I_\gamma = 0.2618\%$) γ -lines of $^{197\text{m}}\text{Hg}$ and 77.35 keV ($I_\gamma = 18.7\%$) γ -line of $^{197\text{g}}\text{Hg}$ for activity calculations.^[63]

Mercury-197m/g radiolabeling studies: A variety of labeling buffers and TLC conditions were screened in [$^{197\text{m/g}}\text{Hg}$]Hg²⁺ labeling studies as described in the Supporting Information; the successful conditions are outlined in detail below. The ligands DOTA, NS₄, NS₄-CA and NS₄-BA were made up as stock solutions (10⁻³ M) in deionized water (in the case of DOTA) or a 10% DMSO-water mixture (in the case of the sulfur-rich chelators). A serial dilution was used to prepare ligand solutions at 10⁻⁴, 10⁻⁵ M, 10⁻⁶ M, and 10⁻⁷ M in water for all chelators. An aliquot (10 μL) of each ligand solution (or water/DMSO, for negative controls) was diluted with ammonium acetate buffer (1 M; pH 7) such that the final reaction volume was 100 μL . [$^{197\text{m/g}}\text{Hg}$]HgCl₂ (1 MBq, 3 μL) was added and mixed gently to begin the radiolabeling reaction at different temperatures. The different concentrations correspond to the following molar activities: 0.01 MBq/nmol (10⁻³ M), 0.1 MBq/nmol (10⁻⁴ M), 1 MBq/nmol (10⁻⁵ M), 10 MBq/nmol (10⁻⁶ M), 100 MBq/nmol (10⁻⁷ M). Radiolabeling reactions were performed at least in triplicate to ensure reproducibility.

The complex formation was monitored for each reaction by acquiring the non-isolated percentage radiochemical yield (%RCY) at varying time points. This was achieved by extracting an aliquot (10 μL) of the reaction solution and adding it to an equal volume of dimercaptosuccinic acid solution (DMSA, 50 mM, pH 5). The quenched solution was gently mixed and analyzed by spotting a portion (10 μL) of the quenched mixture onto the bottom of an iTLC-SG plate (1 cm \times 10 cm, baseline at 1 cm), and then developed using DMSA (50 mM, pH 5) solution. Under these conditions, the [$^{197\text{m}}\text{Hg}$]Hg²⁺-complexes remain at the baseline ($R_f = 0$), while the unchelated [$^{197\text{m/g}}\text{Hg}$]Hg²⁺ migrates upwards with the solvent ($R_f = 1$). TLC plates were analyzed on a BioScan System 200 imaging scanner equipped with a BioScan Autochanger 1000 and WinScan software and radiolabeling yields were calculated by integrating the peaks in the radio-chromatogram.

Glutathione (GSH) competition assay: [$^{197\text{m/g}}\text{Hg}$][Hg(NS₄-BA)]²⁺ (prepared as described above) or radiolabeling controls (water instead of the ligand) were added to a 50 mM L-glutathione solution (1:22 V/V GSH: reaction solution dilution), and the mixtures were incubated at 37 °C. The [$^{197\text{m/g}}\text{Hg}$][Hg(NS₄-BA)]²⁺ complex integrity was monitored over the course of 3 days using iTLC-SG developed with the L-glutathione solution (50 mM). Under these conditions, uncomplexed [$^{197\text{m/g}}\text{Hg}$]Hg²⁺ resulting from GSH chelation travelled to the solvent front ($R_f = 1$) while intact [$^{197\text{m/g}}\text{Hg}$]Hg²⁺-complexed species stick to the baseline ($R_f = 0$).

Human serum stability assay: [^{197m}gHg][$\text{Hg}(\text{NS}_4)$] $^{2+}$ and [^{197m}gHg][$\text{Hg}(\text{NS}_4\text{-BA})$] $^{2+}$ (prepared as described above) or radiolabeling controls (water instead of ligand) were diluted in human serum (1:1 V/V dilution), and the solutions were incubated at 37 °C. The metal-complex stability was monitored over the course of 24 h via sodium dodecyl sulfate–polyacrylamide gel electrophoresis (SDS-PAGE). At each time point, 10 μL of the reaction was taken and mixed with a 10 μL Laemmli sample buffer and was directly loaded onto the SDS-PAGE gels. The SDS-PAGE was run at ambient temperature and 150 V until the dye front reached the resolving gel (1 h). After electrophoresis, the gel was scanned with the radio-TLC scanner described above in order to determine the %intact complex. The same protocol was used with free [^{197m}gHg][Hg] $^{2+}$ and the ^{197m}gHg -complexes diluted in phosphate-buffered saline (PBS) to assess their electrophoretic mobility.

Supporting Information

The Supporting Information is available online free of charge. Experimental ^1H and ^{13}C NMR spectra, mass spectra, DFT data, radio-iTLC chromatograms, labeling and kinetic inertness assay data and protocol details can be found within.

Acknowledgements

Funding for this work was provided by Natural Sciences and Engineering Research Council of Canada (NSERC) Discovery programs [grant numbers RGPIN-2019-07207(CR), RGPIN-2018-04997 (VR), RGPIN-2017-04966 (GS)], Canadian Cancer Society Research Institute (CCSRI) [grant number 706774] and Canadian Institutes of Health Research (CIHR) [grant number: GR021373]. TRIUMF receives federal funding via a contribution agreement with the National Research Council of Canada. We would like to thank Dr. Raymond Reilly and the Reilly Group (University of Toronto) for the insightful discussions. We would also like to thank the TR-13 Cyclotron Operations Group consisting of Toni Epp, Ryley Morgan, Spencer Staiger, and led by David Prevost for regular irradiations of Au targets. M. T. gratefully acknowledges “Fondazione Aldo Gini” of the University of Padova (Italy) for the financial support.

Conflict of Interest

The authors declare no conflict of interest.

Data Availability Statement

The data that support the findings of this study are available from the corresponding author upon reasonable request.

Keywords: Hg · macrocycles · mercury-197 · radiopharmaceuticals · radiometals

[1] E. W. Price, C. Orvig, *Chem. Soc. Rev.* **2014**, *43*, 260–290.

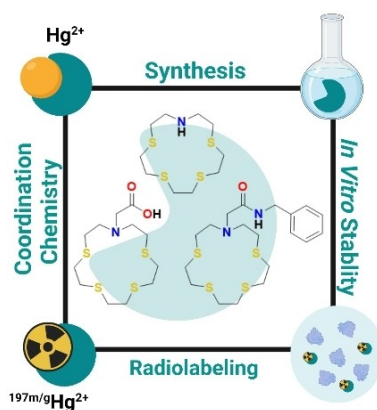
- [2] C. F. Ramogida, C. Orvig, *Chem. Commun.* **2013**, *49*, 4720–4739.
 [3] C. Dong, Z. Liu, F. Wang, *Curr. Med. Chem.* **2013**, *21*, 139–152.
 [4] T. Li, E. C. I. Ao, B. Lambert, B. Brans, S. Vandenberghe, G. S. P. Mok, *Theranostics* **2017**, *7*, 4551–4565.
 [5] P. Randhawa, A. P. Olson, S. Chen, K. L. Gower-fry, C. Hoehr, J. W. Engle, C. F. Ramogida, V. Radchenko, *Curr. Radiopharm.* **2021**, *14*, 1–26.
 [6] J. D. Despotopoulos, K. N. Kmak, D. A. Shaughnessy, *J. Radioanal. Nucl. Chem.* **2018**, *317*, 985–989.
 [7] D. Filosofov, E. Kurakina, V. Radchenko, *Nucl. Med. Biol.* **2021**, *94–95*, 1–19.
 [8] S. Aghevlian, A. J. Boyle, R. M. Reilly, *Adv. Drug Delivery Rev.* **2017**, *109*, 102–118.
 [9] A. Ku, V. J. Facca, Z. Cai, R. M. Reilly, *EJNMMI Radiopharm. Chem.* **2019**, *4*, 27.
 [10] P. Bernhardt, E. Forsell-Aronsson, L. Jacobsson, G. Skarnemark, *Acta Oncol.* **2001**, *40*, 602–608.
 [11] J. Stepanek, B. Larsson, R. Weinreich, *Acta Oncol.* **1996**, *35*, 863–868.
 [12] E. M. Smith, C. C. Harris, R. H. Rohrer, *J. Nucl. Med.* **1966**, *7*, 23–31.
 [13] J. P. Pouget, I. Navarro-Teulon, M. Bardiès, N. Chouin, G. Cartron, A. Pèlerin, D. Azria, *Nat. Rev. Clin. Oncol.* **2011**, *8*, 720–734.
 [14] M. Walther, S. Preusche, S. Bartel, G. Wunderlich, R. Freudenberg, J. Steinbach, H. J. Pietzsch, *Appl. Radiat. Isot.* **2015**, *97*, 177–181.
 [15] X. Huang, C. Zhou, *Nucl. Data Sheets* **2005**, *104*, 283–426.
 [16] S. Warner, *Scientist* **2004**, *18*, 38–39.
 [17] M. Walther, O. Lebeda, S. Preusche, J. Steinbach, *AIP Conf. Proc.* **2017**, *1845*, 020023.
 [18] J. D. Despotopoulos, K. N. Kmak, *J. Radioanal. Nucl. Chem.* **2021**, *327*, 2–7.
 [19] M. M. Ter-pogossian, D. Ph, *J. Nucl. Med.* **1966**, *7*, 50–59.
 [20] M. C. Overton, *Jama* **1965**, *191*, 431.
 [21] D. B. Sodee, *J. Nucl. Med.* **1964**, *5*, 74–75.
 [22] R. R. Borghgraef, R. H. Kessler, R. F. Pitts, *J. Clin. Invest.* **1956**, *35*, 1055–1066.
 [23] J. M. Cappin, D. P. Greaves, *Br. J. Ophthalmol.* **1972**, *56*, 805–811.
 [24] R. Freudenberg, R. Apolle, M. Walther, H. Hartmann, J. Kotzerke, *EJNMMI Phys.* **2018**, *5*, 1–14.
 [25] I. M. F. Gilpin, M. Ullrich, T. Wünsche, K. Zarschle, O. Lebeda, J. Pietzsch, H. J. Pietzsch, M. Walther, *ChemMedChem* **2021**, *16*, 1–6.
 [26] H. J. Pietzsch, M. Walther, T. Wünsche (Helmholtz-Zentrum Dresden-Rossendorf), WO 2018/146116 A1, **2018**.
 [27] P. J. Blower, R. J. Smith, C. Jolley, *Nucl. Med. Commun.* **1992**, *13*, 231.
 [28] R. C. Reba, J. G. McAfee, H. N. Wagner, *Medicine* **1963**, *42*, 269.
 [29] J. A. O'Donoghue, T. E. Wheldon, *Phys. Med. Biol.* **1973**, *41*.
 [30] G. Saha, *Fundamentals of Nuclear Pharmacy*, Springer Science And Business Media LLC, **2013**.
 [31] M. Tosato, M. Asti, M. Dalla Tiezza, L. Orian, D. Häussinger, R. Vogel, U. Köster, M. Jensen, A. Andrighetto, P. Pastore, V. Di Marco, *Inorg. Chem.* **2020**, *59*, 10907–10919.
 [32] T. I. Kostelnik, C. Orvig, *Chem. Rev.* **2019**, *119*, 902–956.
 [33] C. Wang, PhD thesis, Technischen Universität Dresden (Dresden), **2018**.
 [34] T. Chen, W. Zhu, Y. Xu, S. Zhang, X. Zhang, X. Qian, *Dalton Trans.* **2010**, *39*, 1316–1320.
 [35] J. Isaad, A. El Achari, *Tetrahedron* **2013**, *69*, 4866–4874.
 [36] A. Asaduzzaman, D. Riccardi, A. T. Afaneh, C. J. Cooper, J. C. Smith, F. Wang, J. M. Parks, G. Schreckenbach, *Acc. Chem. Res.* **2019**, *52*, 379–388.
 [37] O. A. Gansow, *Int. J. Radiat. Appl. Instrum. Part A* **1991**, *18*, 369–381.
 [38] L. G. A. Van de Water, W. Buijs, W. L. Driessen, J. Reedijk, *New J. Chem.* **2001**, *25*, 243–249.
 [39] M. Tosato, PhD thesis, University of Padua (Padova), **2022**.
 [40] C. F. MacRae, I. Sovago, S. J. Cottrell, P. T. A. Galek, P. McCabe, E. Pidcock, M. Platings, G. P. Shields, J. S. Stevens, M. Towler, P. A. Wood, *J. Appl. Crystallogr.* **2020**, *53*, 226–235.
 [41] T. Lu, S. Manzetti, *Struct. Chem.* **2014**, *25*, 1521–1533.
 [42] T. Lu, F. Chen, *J. Comput. Chem.* **2012**, *33*, 580–592.
 [43] M. Ngu-Schwemlein, J. Merle, T. Cameron, C. Witcher, D. Todd, *Bioorg. Med. Chem.* **2021**, *44*, 116296.
 [44] J. P. Gallivan, D. A. Dougherty, *Proc. Natl. Acad. Sci. USA* **1999**, *96*, 9459–9464.
 [45] W. A. Volkert, T. J. Huffman, *Chem. Rev.* **1999**, *99*, 2269–2292.
 [46] D. A. Dickinson, H. J. Forman, *Biochem. Pharmacol.* **2002**, *64*, 1019–1026.
 [47] D. M. Weekes, C. F. Ramogida, M. D. G. Jaraquemada-Peláez, B. O. Patrick, C. Apte, T. I. Kostelnik, J. F. Cawthray, L. Murphy, C. Orvig, *Inorg. Chem.* **2016**, *55*, 12544–12558.
 [48] E. W. Price, B. M. Zeglis, J. F. Cawthray, C. F. Ramogida, N. Ramos, J. S. Lewis, M. J. Adam, C. Orvig, *J. Am. Chem. Soc.* **2013**, *135*, 12707–12721.
 [49] I. Lisewska, J. Potocki, A. Pasternak, *J. Labelled Compd.* **1972**, *8*, 561–566.

- [50] J. R. Ballinger, *Br. J. Radiol.* **2018**, *91*, 20170969.
- [51] K. Yong, M. Brechbiel, *AIMS Med. Sci.* **2015**, *2*, 228–245.
- [52] T. Hwang, A. J. Shaka, *J. Magn. Reson. Ser. A* **1995**, *112*, 275–279.
- [53] K. J. Powell, P. L. Brown, R. H. Byrne, T. Gajda, G. Hefter, S. Sjöberg, H. Wanner, *Pure Appl. Chem.* **2005**, *77*, 739–800.
- [54] C. T. Wallingford, *Gaussian* **16**, **2016**.
- [55] A. D. Beck, *J. Chem. Phys.* **1993**, *98*, 5648–5656.
- [56] T. Lecklider, *EE Eval. Eng.* **2011**, *50*, 36–39.
- [57] A. D. Becke, E. R. Johnson, *J. Chem. Phys.* **2005**, *123*, 0–9.
- [58] S. Grimme, J. Antony, S. Ehrlich, H. Krieg, *J. Chem. Phys.* **2010**, *132*.
- [59] D. Andrae, U. Häußermann, M. Dolg, H. Stoll, H. Preuß, *Theor. Chim. Acta* **1990**, *77*, 123–141.
- [60] M. D. Hanwell, D. E. Curtis, D. C. Lonie, T. Vandermeersch, E. Zurek, G. R. Hutchison, *J. Cheminf.* **2012**, *4*, 7.
- [61] R. D. Johnson III, NIST Standard Reference Database Number 101, **2020**.
- [62] S. Chen, M. Bas, S. Happel, P. Randhawa, S. Mcneil, S. Zeisler, K. Maskell, C. Hoehr, C. Ramogida, V. Radchenko, *J. Chromatogr. A* **2023**, *1688*.
- [63] “Live Chart of Nuclides. IAEA,” can be found under <https://www.nds.iaea.org/relnsd/vcharhtml/VChartHTML.html/>.

Manuscript received: December 6, 2022
Accepted manuscript online: January 26, 2023
Version of record online: ■■, ■■

RESEARCH ARTICLE

Three sulfur-rich macrocyclic chelators were synthesized; their ability to bind Hg^{2+} was studied. The validity of these chelators for $^{197\text{m/g}}\text{Hg}^{2+}$ radiopharmaceutical incorporation was investigated through radiolabeling studies and in vitro stability assays. The importance of sulfur coordinating atoms was rationalized, thus helping to design $^{197\text{m/g}}\text{Hg}^{2+}$ chelators for nuclear medicine applications.



*P. Randhawa, K. L. Gower-Fry, C. M. K. Stienstra, Dr. M. Tosato, S. Chen, Dr. Y. Gao, Dr. A. W. McDonagh, Prof. Dr. V. Di Marco, Dr. V. Radchenko, Prof. Dr. G. Schreckenbach, Prof. Dr. C. F. Ramogida**

1 – 15

Selective Chelation of the Exotic Meitner-Auger Emitter Mercury-197 m/g with Sulfur-Rich Macrocyclic Ligands: Towards the Future of Theranostic Radiopharmaceuticals

